Supporting Information

Cell membrane disruption by vertical Micro/Nano pillars: the role of membrane bending and traction forces.

Rosario Capozza[a], Valeria Caprettini[a,b], Carlo A. Gonano[a] , Alessandro Bosca[a], Fabio Moia[a], Francesca Santoro[c], Francesco De Angelis[a]*

[a]Istituto Italiano di Tecnologia, via Morego 30, 16163 Genova, Italy

[b]Università degli studi di Genova, Genova, Italy

[c]Center for Advanced Biomaterials for Healthcare, Istituto Italiano di Tecnologia, 80125 Napoli, Italy

*corresponding author's email: francesco.deangelis@iit.it

S1: Fabrication method

S2: Cell culture and imaging

S3. MD simulation of Membrane self-assembly

S4. Strain-stress curve

S5. Bending stiffness

S6. Maximum stress on the membrane's section

S7. Stress-strain relation for bent membrane

S1. Fabrication method

For the fabrication of the silicon pillars arrays, we used first photolithography to pattern a chrome hard mask on a silicon wafer substrate and then dry etching to define the pillars in the silicon bulk using a customized multi-step process to control the shape of the pillars' top edges.

As a first step, 100nm of chrome has been deposited on a <100> N-type silicon wafer using e-beam evaporation (Kurt J. Lesker PVD 75). Then a layer of AZ5214E photoresist has been deposited by spin coating at 6000 RPM, baked at 112°C for 50s, exposed to UV light (dose 45 mJ/cm2) using a SUSS MA-6 Mask Aligner and finally developed using AZ726 developer for 60s. The photo-patterned resist has then been used to define in the chrome layer by wet etching (immersion in Chrome Etch 18 for 45s at 20°C) an array of 2μm-wide discs spaced 6μm center-to center to be used as a hard mask for the subsequent dry etching of the pillars.

Silicon dry etching has been performed in an ICP-RIE reactor (Sentech SI 500) using a customized multi-step silicon etching process based on SF_6 and C_4F_8 gases. In order to obtain pillars with sharp top edges, we used a multi-step process (5 steps, 60s etching time each) at 20°C where the C_4F_8:SF_6 ratio has been gradually increased starting from 2:1 (60:30 sccm) to 3:1 (90:30 sccm); in this way, the top edge of the pillars has been protected from unwanted under-etch during the late steps of the etching. The opposite paradigm has been exploited to obtain pillars where the top edge has been consumed in the final steps of the process (smooth edges), while the pillar bodies stayed untouched with vertical side-walls. In this case, C_4F_8:SF_6 ratio has been kept at 4:1 (60:15 sccm) the first two 60s steps, and then decreased to 3:1 (45:15 sccm). For both the above-mentioned processes, ICP source has been set at 1200W, RF power at 20W and reactor pressure at 1.33 Pa. After dry etching, any residual of chrome has been removed using Chrome Etch 18.

SEM images have been acquired with a dual beam Helios Nanolab 650 by ThermoFisher using a current of 0.20nA and a beam acceleration of 10kV. A sacrificial layer of platinum has been deposited on the pillars to perform the cross sections and evaluate the curvature radius of the nanostructures.

Figure S1 shows a blow-up of a smooth pillar (refer to Figure 5b), displaying sharp local asperities.

The permeabilization likelihood is mostly affected by the overall geometry of the pillar's edge, while local asperities play a minor role.
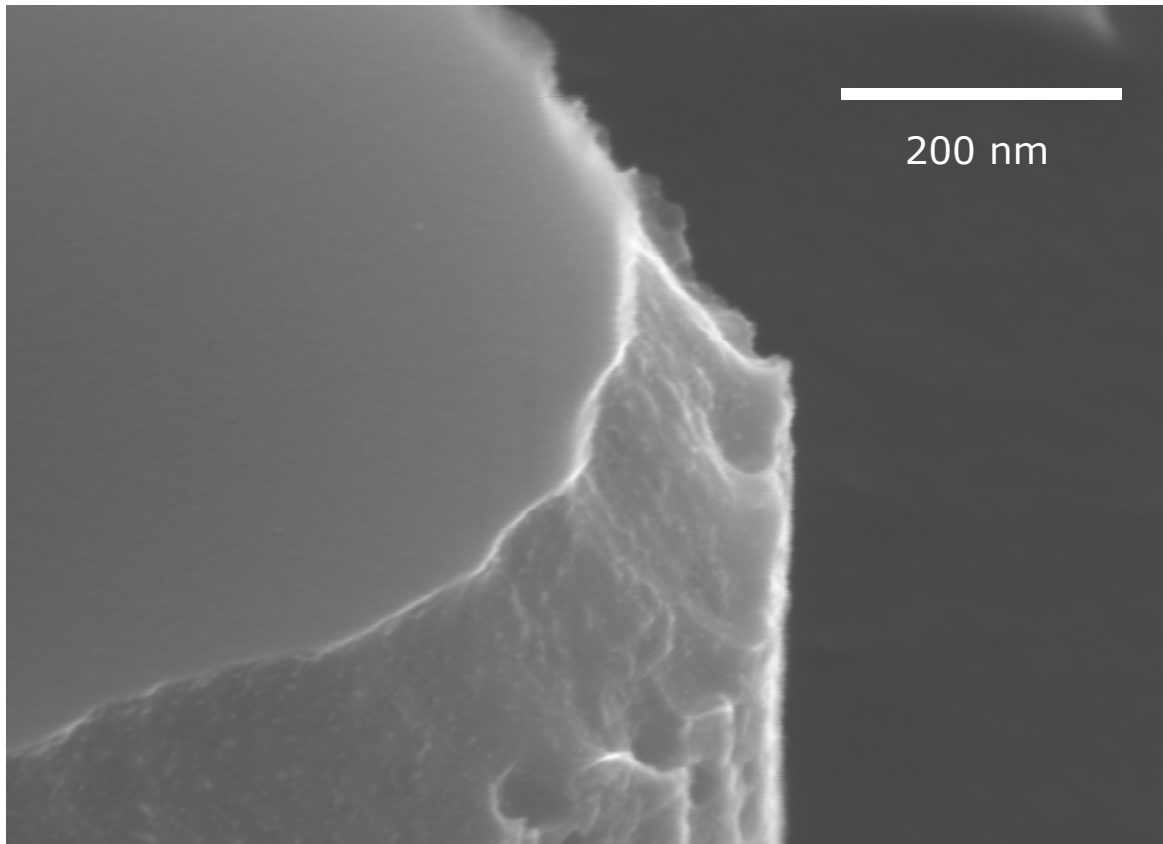
Figure S1. SEM image of a "smooth" pillar with diameter of 2 μm, height of 1 μm showing a detail of the edge. The estimated "overall radius of curvature" is $R_{smooth} \sim 250 \pm 20$ nm.

One of the image in the TOC represents a critical point dried NIH-3T3 cell culture grew on a 3D nanostructured substrate with sharp edge pillars. The cells have been fixed in a solution of 2.5% gluta, dehydrated with increased concentration of ethanol, and then dried using a critical point dried (CPD). This technique allows removing all the liquid from a sample without generating any superficial tension on it, thus preserving the external features of the biological specimen. This is possible by substituting liquid CO_2 to the liquid of the sample (in our case ethanol), and then rising the temperature above the critical temperature (35°C) maintaining the pressure below 1200psi. In this way, the CO_2 change phases and become vapor without changing its density, avoiding surface tension effects that can affect the cell morphology. For clarity, we report an image obtained with the described technique in Fig.S2. It depicts a cell in adhesion with the substrate, tightly wrapping around the sharp pillar head.
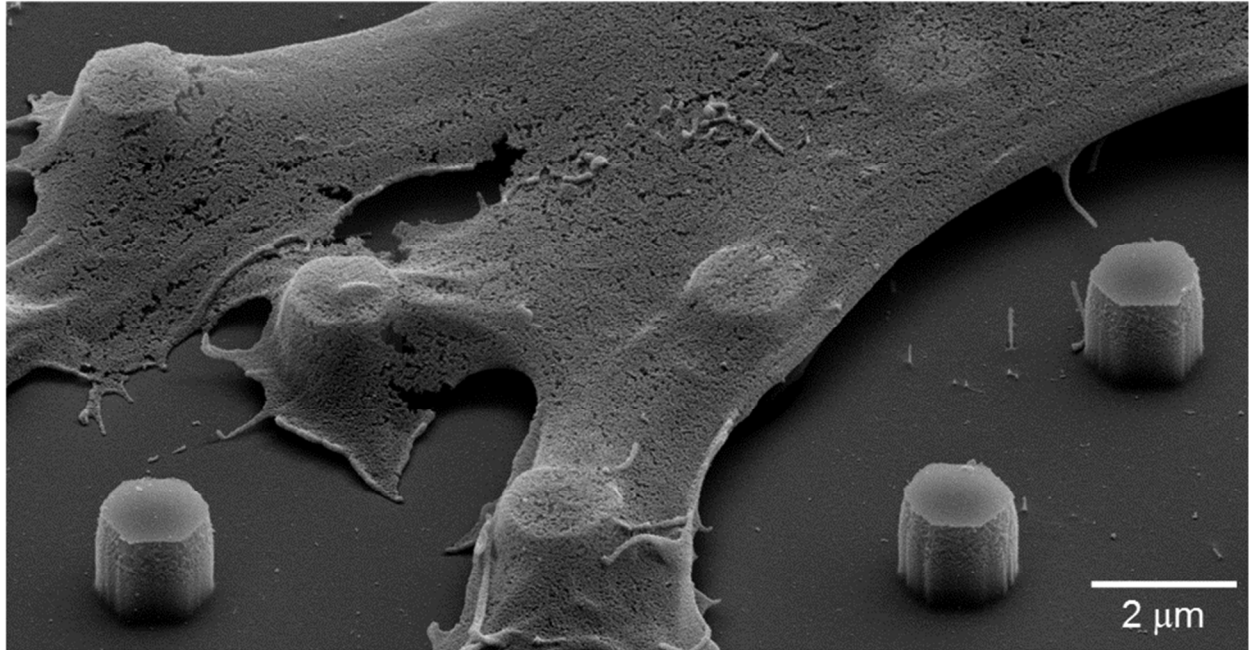
Figure S2. Image showing a cell sitting on a vertical array of sharp pillars, obtained by critical point dryer (CPD) technique. The cell is in adhesion with the substrate, tightly wrapping around the pillar head.

S2. Cell culture and imaging

The cells that appear in Figures 1 and 5 are NIH-3T3 plated with a density of $1{,}5 \times 10^4$ cell/cm^2 in DMEM complemented with 1% penicillin streptomycin antibiotics and 10% inactivated fetal bovine serum (FBS); cells are incubated at controlled temperature, humidity and CO_2 concentration for 48h. A viability test has been performed and both calcein AM and propidium iodide (2μM) have been administer to the cultures. Calcein AM is a membrane permeable molecule that becomes fluorescent only when enters in living cells, while propidium iodide is a membrane impermeable dye that becomes red when it inserts in between the DNA double strand. After 20 minutes of incubation, the samples have been washed three times with PBS and then analyzed through a fluorescence microscope. The fluorescent images are taken by an upright Ecplise FN-1 microscope from Nikon with a 20x air objective with long working distance. The images are recorded by a Nikon fluorescent camera and the fluorophore is excited with a Nikon TRITC filter and a Nikon FITC filter. Images have been processed and the different color channel have been merged with Gimp2.0.

Figure 1a is a SEM image of a NIH-3T3 cell cross section. The cells have been fixed and stained using a recently implemented RO – T – O procedure[1] and samples have been infiltrated

increasing concentration of resin in ethanol. The excess of resin have been removed prior to polymerization in order to allow the detection of the cells on the 3D nanostructures using SEM[1]. FIB/SEM cross section images have been made with a FEI Helios Nanolab 650 dual beam microscope. A 1μm layer of Pt has been deposited on the selected region by a Gas Injection System (GIS) integrated to the microscope before the cutting. An initial cut was made with a high current (9.3nA) of the ionic beam, and then a cleaning cross section was performed using a 0.79 nA ion current with a 30.0kV accelerating voltage. The imaging was made using the immersion mode of the microscope and backscattered electrons have been detected with TLD detector.
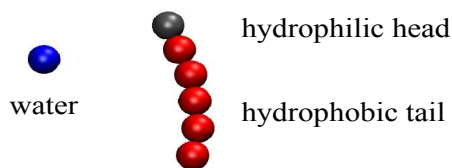
S3. MD simulation of Membrane self-assembly

We performed Molecular Dynamics simulations of a lipid bilayer in water by using Langevin dynamics that allows to calculate not only the forces due to bending, but also to the thermal fluctuations. Periodic boundary conditions were imposed in all directions and the temperature was kept at 301.7 K by means of a Langevin thermostat applied to all particles.

In our numerical simulations, we assume the existence of three types of particles: "water-like" particles (w), hydrophilic "head" particles (h), and hydrophobic "tail" particles (t). A water molecule is approximated as a single "w" particle, while a lipid molecule is composed of one "h" particle and five "t" particles joined together by harmonic interactions.

The three types of particles interact by means of Lennard-Jones potentials ϕ_{ij}, with energy parameter ϵ_{ij} and distance parameter λ_{ij}:

$$\phi_{ij}(r) = 4\epsilon_{ij}\left[\left(\frac{\lambda_{ij}}{r}\right)^{12} - \left(\frac{\lambda_{ij}}{r}\right)^{6}\right]$$

The indices i, j indicate the type of atom (w, h or t) and r is the distance between the atoms. We have assumed that for all the interactions $\epsilon_{ij} = 6.94 \cdot 10^{-21} J$ except for $\epsilon_{tt} = 11.8 \cdot 10^{-21} J$, while $\lambda_{ij} = \lambda = 0.4456 \, nm$ for all interactions. All interactions are truncated at $R_{ij}^c = 2.5\lambda$, except for w-t and h-t interactions where $R_{ij}^c = 2^{1/6}\lambda = 0.5nm$, which makes the latter interactions completely repulsive.

hydrophilic head

water

hydrophobic tail

Equilibrium configuration

t = 100 ps   t = 10 ns
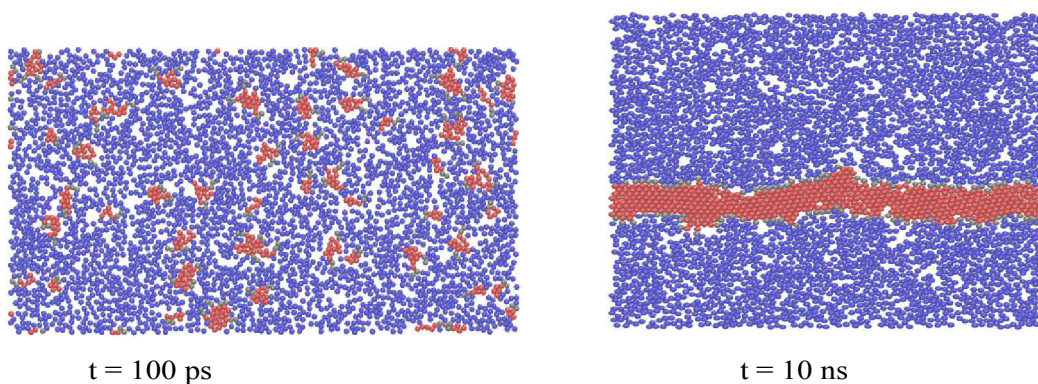
Figure S3 Molecular structure and membrane self-assembly

All simulations have been executed using the LAMMPS package for large scale molecular dynamics simulations. Configurations were stored every 3 ps for further structural and dynamic analyses.

Because of assigned interactions, the heads tend to stay in contact with water (hydrophilic) while tails keep distance from water (hydrophobic) and "segregate" together. Fig.S3 shows two system configurations obtained after t=100 ps and t=10 ns, starting from lipids randomly distributed in water. The equilibrium configuration is clearly a lipid bilayer with thickness of $l_y \approx 4.5 nm$ and average distance between hydrophilic heads $d_{eq} \approx 0.83\ nm$. Considering that our 2D simulation geometry is a single atomic sheet of depth of $l_z = 0.5 nm$ (in the z direction), the transversal area is $A_t = 2.25\ nm^2$.

The equilibrium configuration of the membrane can be predicted estimating the two-dimensional "Shape factor", $S_f = A_c/(a_h \cdot l_t)$, where A_c is the area of hydrocarbon chains, a_h is the head thickness, and l_t is the tail length. It is easily shown that $S_f \leq 1/2$ for a micelle, while in our case $S_f \approx 1$ and we have indeed a bilayer.

S4. Strain-stress curve

When the cell membrane undergoes large deformation, the approximation of linear material is no longer valid and the membrane could also exhibit a plastic behavior. In this case the Young's modulus can be interpreted as the derivative of stress σ with respect to the strain ε, formally:

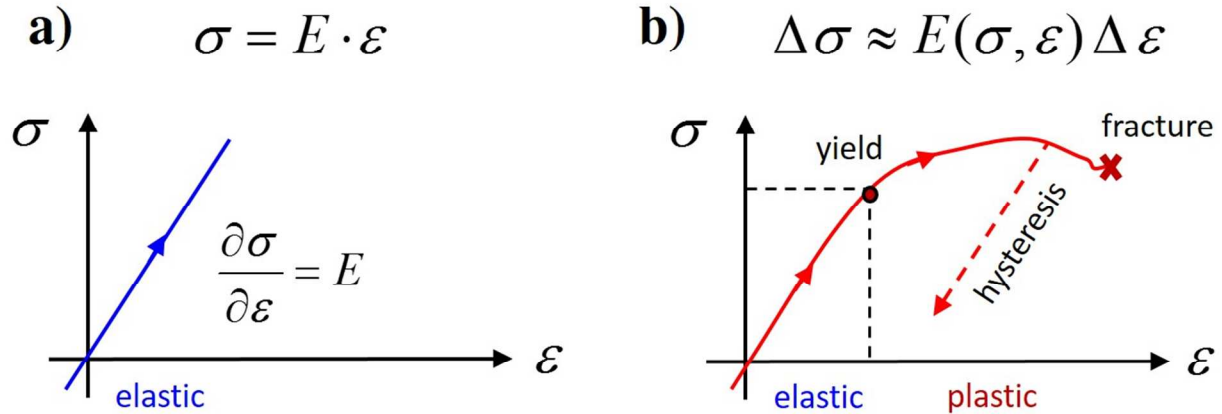$$\Delta\sigma = E(\sigma, \varepsilon) \cdot \Delta\varepsilon$$

a) $\sigma = E \cdot \varepsilon$ $\qquad$ **b)** $\Delta\sigma \approx E(\sigma, \varepsilon)\Delta\varepsilon$

Figure S4. a) Strain-stress curve for an ideal linear material. b) Strain-stress curve for a non-linear, hysteretic material

S5. Bending stiffness

The bending moment M_z at the membrane's center can be easily calculated from the forces on cylinders and their application points. For a linear material, the bending moment is proportional to the local curvature 1/R through the Young modulus's:

$$M_z = EJ\frac{1}{R} \approx EJ\frac{\partial^2 s_y}{\partial x^2}$$

where J is the 2nd moment of area of the membrane's cross-section and s_y is the vertical displacement at the center of the membrane.

In similar way, the bending stiffness K_{bend} links the moment per unit of depth (M_z/l_z) to the curvature:

$$\frac{M_z}{l_z} = K_{bend}\frac{1}{R} \approx K_{bend}\frac{\partial^2 s_y}{\partial x^2}$$

Hence, K_{bend} can be expressed as:

$$K_{bend} = \frac{EJ}{l_z}$$

For a rectangular section, with thickness l_y and depth l_z, the quantities J and K_{bend} turn out to be:

$$J = \frac{1}{12} l_z l_y^3; \qquad K_{bend} = \frac{1}{12} E l_y^3$$

We highlight that K_{bend} is proportional to the Young's modulus and to the cube of membrane's thickness, while the Young's modulus E does not depend on any geometrical parameter.

S6. Maximum stress on the membrane's section

Since the membrane is inflected in the y-x plane, the stress distribution on its section is not uniform. Assuming the stress σ does not vary in the z direction, the bending moment on the whole section can be calculated as:

$$M_z = l_z \int_{y_G - l_y/2}^{y_G + l_y/2} \sigma_x(y) \cdot (y - y_G) \, dy$$

where y_G here coincide with the center of the section.

For pure bending, the membrane's upper border is stretched, while the lower one is compressed. Usually the stress distribution is assumed to be linear (see Figure S4), thus it can be expressed as:

$$\sigma_x(y) = \sigma_{x,max} \cdot \left(\frac{y - y_G}{l_y / 2} \right)$$

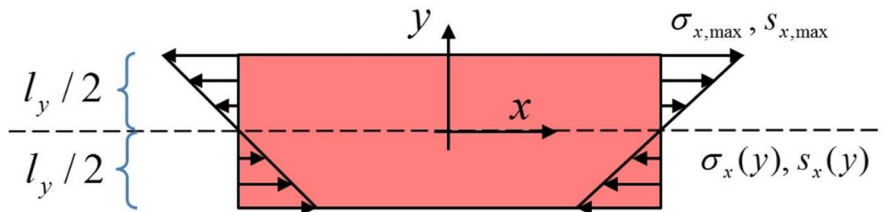where $\sigma_{x,max}$ is the maximum stress on the section.

Figure S5. Linear displacement $s_x(y)$ and stress $\sigma_x(y)$ distributions on a beam element, subjected to a pure bending moment M_z

Joining together the equation for J, M_z and σ_x, it yields the relation linking the bending moment and the maximum stress:

$$\sigma_{x,\max} = \frac{1}{2}\frac{l_y}{J}M_z = \frac{6}{l_y^2 l_z}M_z$$

Since either the moment or the geometry are known, we use this equation for estimating the maximum stress.

S7. Stress-strain relation for bent membrane

For a linear material the stress and the local curvature are both proportional to the bending moment. It is then possible to show that the stress-strain relation reads as:

$$\sigma_{x,\max} = E \cdot \left(\frac{l_y/2}{R} \right) = E \cdot \varepsilon_{xy,\max}$$

Since both the maximum stress and the curvature strain ε_{xy} can be obtained from the simulations, even for a non linear material the Young's modulus can be estimated as:

$$E \approx \frac{\Delta\sigma_{x,\max}}{\Delta\varepsilon_{xy,\max}}$$

References

1. F. Santoro, W. Zhao, L.-M. Joubert, L. Duan, J. Schnitker, Y. van de Burgt, H.-Y. Lou, B. Liu, A. Salleo, L. Cui, Y. Cui and B. Cui, Revealing the Cell–Material Interface with Nanometer Resolution by Focused Ion Beam/Scanning Electron Microscopy. *ACS Nano* **11,** 8320–8328 (2017).